Journal of Computational and Applied Mathematics 234 (2010) 1670–1677

Contents lists available at ScienceDirect

Journal of Computational and Applied Mathematics

journal homepage: www.elsevier.com/locate/cam

A comparison of NRBCs for PUFEM in 2D Helmholtz problems at high wave numbers

O. Laghrouche [a,*], A. El-Kacimi [a], J. Trevelyan [b]

[a] School of the Built Environment, Heriot-Watt University, Edinburgh EH14 4AS, UK

[b] School of Engineering, Durham University, Durham DH1 3LE, UK

ARTICLE INFO

Article history:
Received 23 November 2007
Received in revised form 11 April 2008

Keywords:
Helmholtz equation
Finite elements
Plane wave basis
Non-reflecting boundary conditions
Wave scattering

ABSTRACT

In this work, exact and approximate non-reflecting boundary conditions (NRBCs) are implemented with the Partition of Unity Finite Element Method (PUFEM) to solve short wave scattering problems governed by the Helmholtz equation in two dimensions. By short wave problems, we mean situations in which the wavelength is a small fraction of the characteristic dimension of the scatterer. Various NRBCs are implemented and a comparison of their performance is carried out based on the accuracy of the results, ease of implementation and computational cost. The aim is to accurately model such problems in a reduced computational domain around the scatterer with fewer elements and without refining the mesh at each wave number.

1. Introduction

To solve wave scattering problems in unbounded media using the finite element method, it is necessary to truncate the domain at some boundaries, to form the computational domain, and to apply a suitable boundary condition allowing the outgoing waves to radiate away towards infinity. If approximate boundary conditions are used, these should be placed at a sufficiently large distance from the scatterer, which leads to solutions in large computational domains. If, however, accurate boundary conditions are used, the computational domain can be reduced so that the truncation boundary is very close to the scatterer and hence fewer finite elements may be used. But exact NRBCs are non-local and, as a consequence, the global system becomes dense near the outer boundary.

Another problem arises from the fact that polynomial based finite elements have limited ability to deal with short wave problems due to the requirement of around ten nodal points per wavelength, or even higher resolution for short wave problems. To overcome this difficulty, various finite elements which incorporate knowledge about the problem to be solved were developed. The approach is based on the enrichment of the solution space by analytical solutions. In the case of the Helmholtz equation, plane waves were used with finite elements in the Partition of Unity Method [1–5], Least-Squares Method [6], Ultra-Weak Variational Method [7,8] and Discontinuous Enrichment method [9,10]. The reader is directed to reference [11] for a survey of the activity which took place up to 2004. More recent work could be found, for example, in [12,13]. The developed plane wave basis finite elements have been very successful in reducing the computing effort by up to 90% [14,15] and it is demonstrated that a discretization level of about 2.5 degrees of freedom per wavelength is sufficient to achieve engineering accuracy [12,16].

In this work, plane wave basis finite elements are combined with exact and approximate models of NRBCs to solve wave scattering problems. The problem of interest is a simple model of an acoustic plane wave scattered by a rigid circular cylinder,

* Corresponding author.
E-mail address: O.Laghrouche@hw.ac.uk (O. Laghrouche).

0377-0427/$ – see front matter © 2009 Elsevier B.V. All rights reserved.
doi:10.1016/j.cam.2009.08.014

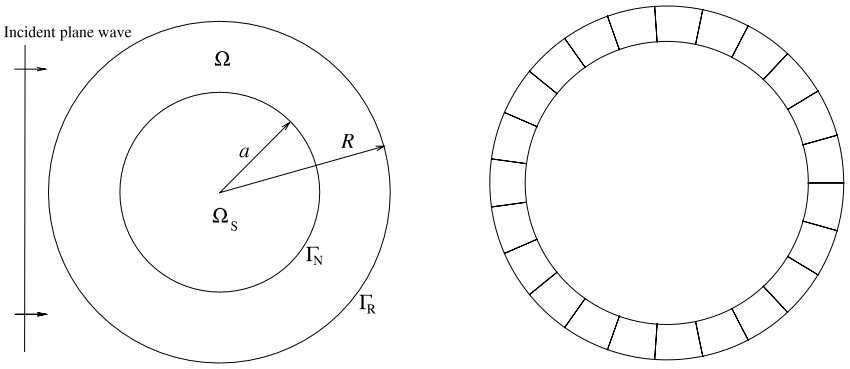

Fig. 1. (left) Schematic diagram of the scattering problem, (right) Mesh of the computational domain.

for which the exact solution is known. Various numerical tests are carried out with a fixed mesh and for a wide range of wave numbers. Three approximate boundary conditions are used. Those are of Bayliss, Gunzburger and Turkel (BGT) [17,18], Engquist and Majda (EM) [19,20], and Feng (F) [21]. Different orders of these boundary conditions are also considered. The DtN map is used as an exact NRBC whereas an inhomogeneous Robin condition, through which the analytical solution of the scattering problem is imposed on the outer boundary of the domain, is used as a reference. Note that approximate NRBCs have been developed since the late 1970s and a huge literature is available in this field. Regarding the DtN method, it goes back to Keller and Givoli [22] who developed it for the Helmholtz equation when the outer boundary is a circle or a sphere. It is a non-local condition and it involves an infinite trigonometric or spherical harmonic series. DtN conditions were derived for various equations and geometries, and also for single or multiple disjoint computational domains [23]. So much activity has been taking place in this area and the reader is directed to references [24–28].

2. Formulation of the problem and finite element model

The problem of a horizontal plane wave of potential $u_I = \mathrm{e}^{\mathrm{i}kx}$ scattered by a rigid object Ω_S of boundary Γ_N in an infinite 2D medium is considered. The diffracted potential u satisfies the Helmholtz equation

$$\nabla^2 u + k^2 u = 0 \quad \text{outside } \Omega_S, \tag{1}$$

with the Neumann boundary condition

$$\nabla u \cdot \boldsymbol{n} = -\nabla u_I \cdot \boldsymbol{n} \quad \text{on } \Gamma_N, \tag{2}$$

and the Sommerfeld radiation condition

$$\lim_{r\to\infty} r^{\frac{1}{2}} \left(\frac{\partial u}{\partial r} - \mathrm{i}ku \right) = 0, \tag{3}$$

where ∇^2 denotes the Laplacian operator, ∇ is the gradient vector operator, k is the wave number, $\boldsymbol{n}$ is the outward normal vector to the line boundary Γ_N and i is the complex imaginary such that $\mathrm{i}^2 = -1$. The time variable is removed by considering a harmonic steady state. For computational purpose, the region of interest Ω around the scatterer is bounded by an artificial circular boundary Γ_R of radius R at which special conditions must be imposed to appear transparent to the propagating waves (Fig. 1 (left)). The solution of the original scattering problem is approximated by the solution u of the problem defined by the Helmholtz equation (1) in Ω, the Neumann boundary condition (2) and the boundary condition

$$\nabla u \cdot \boldsymbol{n} - Bu = 0 \quad \text{on } \Gamma_R, \tag{4}$$

where B is an operator corresponding to a NRBC.

Multiplying the Helmholtz equation (1) by a test function v and integrating by parts, we obtain a weak formulation of the problem where it is required to find the scattered potential $u \in H^1(\Omega)$ such that

$$\int_\Omega \left(\nabla u \cdot \nabla v - k^2 uv \right) \mathrm{d}\Omega - \int_{\Gamma_R} vBu \mathrm{d}\Gamma_R = -\int_{\Gamma_N} v \nabla u_i \cdot \boldsymbol{n} \mathrm{d}\Gamma, \tag{5}$$

for all $v \in H^1(\Omega)$, where $H^1(\Omega)$ is the usual Sobolev space [29]. An existence and uniqueness results for (5) can be established, under appropriate assumptions, by virtue of Fredholm's alternative theorem [30] and continuation arguments [31].

The computational domain Ω is meshed into n-noded finite elements and the potential field u is written as combination of m plane waves as follows

$$u = \sum_{p=1}^{n} \sum_{q=1}^{m} N_p \exp(\mathrm{i}k\boldsymbol{r} \cdot \boldsymbol{d}_q) A_{p,q}, \tag{6}$$

where N_p are the usual polynomial shape functions. The coefficients $A_{p,q}$ are the amplitudes of the set of plane waves associated with each node p. The plane waves are chosen to be evenly distributed such that $\boldsymbol{d}_q = (\cos\alpha_q, \sin\alpha_q)^{\mathrm{T}}$ with $\alpha_q = 2\pi q/m$. The geometry of each finite element is described by the coordinate transformation $\boldsymbol{r} = \mathcal{T}(\boldsymbol{\xi})$ between the global coordinates $\boldsymbol{r} = (x, y)$ and the local coordinates $\boldsymbol{\xi} = (\xi, \eta) \in [-1, 1]^2$. In this work, Galerkin weighting is used and hence the test functions v take the form of the plane wave enriched shape functions. For the evaluation of element matrices, high order Gauss–Legendre integration scheme is used in all computations. Let us recall that semi-analytical integration rules were developed for finite elements with straight edges [32] but were not used in this work because the mesh of the computational domain contains elements with curved edges (Fig. 1 (right)).

3. Non-reflecting boundary conditions considered

All considered NRBCs are briefly presented in this section. Their explanation is beyond the scope of this paper and the reader is directed to the corresponding literature. Note that, through the Robin type boundary condition, the analytical solution of the scattering problem is explicitly imposed on the outer boundary Γ_R. Therefore the corresponding numerical solution will be considered as a reference solution and will provide information on the PUFEM discretization error. It will, therefore, allow to distinguish the contribution of the considered NRBCs to the global error.

3.1. Robin type boundary condition—reference solution

The considered scattering problem by a rigid circular cylinder of radius a has an analytical solution. It is given in [33]

$$\tilde{u} = -\sum_{n=0}^{\infty} \mathrm{i}^n \varepsilon_n \frac{J_n'(ka)}{H_n'(ka)} H_n(kr)\cos n\theta, \tag{7}$$

where r and θ are the polar coordinates of a considered point. H_n and J_n are, respectively, the Hankel function and the Bessel function of the first kind and order n. The prime in H_n' and J_n' denotes differentiation with respect to the argument. The sequence $\{\varepsilon_n\}$ is defined by $\varepsilon_0 = 1$, $\varepsilon_n = 2$ for all $n \geq 1$. The solution (7) is imposed on the outer boundary Γ_R through the Robin boundary condition

$$\nabla\tilde{u} \cdot \boldsymbol{n} + \mathrm{i}k\tilde{u} = g, \tag{8}$$

where g is the boundary condition such that the exact solution of the problem corresponds to the diffracted potential $\tilde{u}$. In this case, the weak formulation of the scattering problem becomes

$$\int_{\Omega} \left(\nabla u \cdot \nabla v - k^2 uv\right) \mathrm{d}\Omega + \int_{\Gamma_R} \mathrm{i}kuv \,\mathrm{d}\Gamma = -\int_{\Gamma_N} v\nabla u_I \cdot \boldsymbol{n} \,\mathrm{d}\Gamma + \int_{\Gamma_R} vg \,\mathrm{d}\Gamma. \tag{9}$$

3.2. Exact boundary condition: DtN

Outside the outer boundary Γ_R the solution u of the scattered potential is expressed as a series sum of harmonics [22]

$$u(r,\theta) = \frac{1}{\pi}\sum_{n=0}^{\infty} \varepsilon_n \frac{H_n(kr)}{H_n(kR)} \int_0^{2\pi} u(R,\theta')\cos n(\theta-\theta')\mathrm{d}\theta'. \tag{10}$$

This time, the sequence $\{\varepsilon_n\}$ is defined by $\varepsilon_0 = \frac{1}{2}$, $\varepsilon_n = 1$ for all $n \geq 1$ and θ' is a reference angle. Considering the normal derivative of expression (10) along the outer boundary Γ_R it is possible to establish the following relation

$$Bu = \frac{k}{\pi}\sum_{n=0}^{N} \varepsilon_n \frac{H_n'(kR)}{H_n(kR)} \int_0^{2\pi} u(R,\theta')\cos n(\theta-\theta')\mathrm{d}\theta', \tag{11}$$

which is the DtN boundary condition. The infinite series of the DtN boundary condition is truncated at N and is then no longer exact. In this case, the DtN map will represent the wave harmonics exactly up to the truncation number. Harari and Hughes [27] derived a simple relation between the number N of terms retained in the series and the non-dimensional wave number kR to ensure the uniqueness of the solution, that is $N \geq kR$. It is also possible to use the modified DtN operator introduced in [26], which removes the difficulties due to the truncation of the infinite series and improves the accuracy regardless of kR and N. In this work, the rule proposed in [27] is used to truncate both expressions (7) and (10).

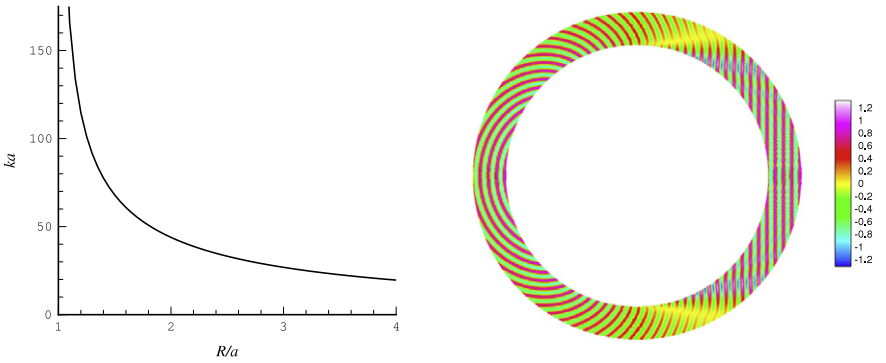

Fig. 2. (left) Non-dimensional wave number ka versus the extent R/a of the computational domain around a circular scatterer for a given mesh resolution, (right) Real part of the diffracted potential, $ka = 100$, $\lambda/a = 0.06$, $\tau = 3$, $\epsilon_2 = 0.1\%$.

3.3. Approximate NRBCs

As mentioned earlier, the three approximate NRBCs considered are of Bayliss, Gunzburger and Turkel of order 1 and 2 (BGT1 and BGT2), Engquist and Majda of order 2 (EM2), and Feng of order 2 and 3 (F2 and F3). The corresponding operator B for each boundary condition and for a considered order is given by

$$\text{BGT1} \quad \mathrm{i}k - \frac{1}{2R}, \tag{12}$$

$$\text{BGT2} \quad \frac{1}{2}\left(\mathrm{i}k - \frac{1}{R}\right)^{-1}\left(2k^2 + \frac{3\mathrm{i}k}{R} - \frac{3}{4R^2} + \frac{1}{R^2}\frac{\partial^2}{\partial^2\theta}\right), \tag{13}$$

$$\text{EM2} \quad \mathrm{i}k - \frac{1}{2R} - \frac{1}{2k^2R^2}\left(\mathrm{i}k + \frac{1}{R}\right)\frac{\partial^2}{\partial^2\theta}, \tag{14}$$

$$\text{F2} \quad \mathrm{i}k - \frac{1}{2R} - \frac{\mathrm{i}}{8kR^2}\left(1 + 4\frac{\partial^2}{\partial^2\theta}\right), \tag{15}$$

$$\text{F3} \quad \mathrm{i}k - \frac{1}{2R} - \frac{1}{8k^2R^2}\left(\mathrm{i}k + \frac{1}{R}\right)\left(1 + 4\frac{\partial^2}{\partial^2\theta}\right). \tag{16}$$

Note that the first order operators due to Engquist and Majda (EM1), and due to Feng (F1) coincide with the BGT1. Higher orders than those mentioned in (12)–(16) are not suitable for finite element implementation due to regularity requirement. Regarding the evaluation of the boundary integral along Γ_R in expression (5), which involves a partial second derivative of the unknown potential u with respect to the angular coordinate θ, it is treated as a second order total derivative and hence the integration by part (17) is possible provided that Γ_R is a closed curve. In this case, it is a circle of radius R.

$$\int_{\Gamma_R} v\frac{\partial^2 u}{\partial\theta^2}\mathrm{d}\Gamma_R = -\int_{\Gamma_R}\frac{\mathrm{d}v}{\mathrm{d}\theta}\frac{\mathrm{d}u}{\mathrm{d}\theta}\mathrm{d}\Gamma_R. \tag{17}$$

4. Numerical results and discussion

The computational domain Ω is meshed into a single layer of 23 finite elements around the scattering cylinder (Fig. 1 (right)). The finite elements are 9-noded and their geometry is interpolated using Lagrange polynomials. At each nodal point we use 30 plane waves to approximate the scattered potential. We define the parameter τ as the number of degrees of freedom (DOF) per wavelength in the problem. It is given by

$$\tau = \frac{2}{k}\sqrt{\frac{\pi n_{\text{tot}} m}{R^2 - a^2}}, \tag{18}$$

where n_{tot} is the total number of nodal points used to mesh the computational domain Ω. Using expression (18) and for a chosen value of the parameter $\tau = 3$, the non-dimensional wave number ka is plotted as a function of the extent of the computational domain R/a. Fig. 2 (left) shows, if the outer boundary Γ_R is very close to the scatterer, it is possible to consider high wave numbers in the problem. For example, for $R/a < 1.25$, it is possible to consider $ka > 100$. However, for a large domain extent, such as $R/a > 2$, for the mesh resolution and plane wave enrichment used here, only low wave numbers could be considered, $ka < 50$.

Table 1
L_2 error corresponding to different boundary conditions on Γ_R.

ka	τ	ϵ_2 [%] Robin	ϵ_2 [%] DtN	ϵ_2 [%] BGT1	ϵ_2 [%] BGT2	ϵ_2 [%] EM2	ϵ_2 [%] F2	ϵ_2 [%] F3
1	304	0.00099	0.00086	20.9	2.3	19	37	28
2	152	0.0014	0.0017	20.4	3.9	6.3	19	8.2
4	76	0.0025	0.0031	18.2	5.0	4.5	9.9	4.5
8	38	0.0056	0.0056	17.2	4.8	4.7	6.0	4.6
10	30	0.0073	0.0073	17.3	4.7	4.6	5.4	4.6
20	15	0.018	0.018	18.4	4.0	3.9	4.2	3.9
30	10	0.033	0.033	17.0	3.5	3.5	3.6	3.5
40	7.6	0.034	0.035	15.6	3.3	3.3	3.3	3.3
50	6.1	0.045	0.043	17.2	3.2	3.2	3.3	3.2
60	5.1	0.049	0.049	15.6	3.1	3.1	3.1	3.1
70	4.3	0.059	0.059	16.0	3.1	3.1	3.1	3.1
80	3.8	0.068	0.067	16.5	3.1	3.1	3.1	3.1
90	3.4	0.075	0.074	15.4	3.0	3.0	3.0	3.0
100	3.0	0.11	0.12	16.6	3.0	3.0	3.0	3.0
110	2.8	0.19	0.20	16.0	3.0	3.0	3.0	3.0
120	2.5	0.24	0.41	15.8	3.0	3.0	3.0	3.0

For the following numerical tests, the computational domain extent is chosen such that $1 \leq R/a \leq 1.25$, which allows us to consider wave numbers $ka \geq 100$. To measure the accuracy of the numerical solution u, we define the L_2 norm error $\epsilon_2 = \|u - \tilde{u}\|_{L_2(\Omega)}/\|\tilde{u}\|_{L_2(\Omega)} \times 100\%$, where $\tilde{u}$ is the exact solution. Fig. 2 (right) shows an example of contour plots of the real part of the scattered potential around the cylinder for $ka = 100$ when the DtN boundary condition is used on the outer boundary Γ_R. In this case, 60 integration points are employed per element, in each spatial direction, for the evaluation of the element matrices. The L_2 error is very satisfactory, $\epsilon_2 = 0.1\%$.

Now, the same scattering problem is considered with the parameters taken above and for a range of wave numbers extending from $ka = 1$ to $ka = 120$. The accuracy of the numerical results is estimated for different boundary conditions applied on Γ_R and the results are summarised in Table 1. First, it is obvious that the DtN boundary condition performs well for all wave numbers. Its performance is very similar to that of the Robin boundary condition, in which the analytical solution is imposed on Γ_R. This proves that the error generated by the DtN boundary condition is negligible and that the L_2 error is due only to the PUFEM discretization. However, L_2 errors generated by all approximate NRBCs show that their contribution to the error, as boundary conditions, is significant compared to the discretization error.

It is worth mentioning that at low wave numbers, the parameter τ indicates that the number of DOF per wavelength is very high, which leads to a high condition number. Despite this fact, the L_2 error stays very low [15]. Also, at low wave numbers, the diameter d of the scattering cylinder is only a fraction of the wavelength λ ($d = 0.32\lambda$ for $ka = 1$). But as the wave number increases, the scatterer's diameter becomes multi-wavelength sized ($d = 3.2\lambda$ for $ka = 10$ and $d = 32\lambda$ for $ka = 100$) and the problem becomes a short wave scattering one. As the finite elements span many wavelengths, for the numerical evaluation of the element matrices, the number of integration points was increased to accommodate the oscillatory behaviour of the integrand. For $ka = 10$, only 10 integration points were used. However, this number was increases to 70 for $ka = 120$.

Regarding the approximate NRBCs, it is clear that BGT1 performs poorly for all wave numbers as the L_2 error remains higher than 15% all the time while using BGT2 leads to a significant drop in ϵ_2. Up to $ka = 20$, BGT2 leads to a better accuracy compared to other approximate NRBCs (EM2, F2 and F3). However, for $ka > 20$, their performances are very similar. At low wave numbers, the distance between the inner boundary Γ_N and the outer boundary Γ_R is very small, in term of the wavelength. But for increasing wave number, this distance becomes very large in term of λ. This is obvious from the simple relationship $(R - a)/\lambda = k/8\pi$. Despite the fact that Γ_R is very far from the scatterer in term of λ, at high wave numbers, the L_2 error remains around 3%. This is due to Γ_R which is not at an asymptotic distance from the scatterer.

Let us recall that Shirron [34] compared the approximate NRBCs considered here for polynomial based finite elements. Canonical problems for rigid scattering were solved where each component of the Anger–Jacobi expansion of the incident plane wave was considered separately. In a different work, Shirron et al. [35] compared these approximate NRBCs and infinite elements for exterior Helmholtz problems where each wavelength was modelled with 16 cubic elements. The computational domain was truncated at a circle of radius $R = a + \lambda$, which means that the outer boundary gets closer to the scatterer as the wave number increases.

To further investigate the efficiency of the NRBCs considered in this work, several tests were carried out for the same scattering problem with the outer boundary Γ_R being all the time 5λ far from the inner boundary Γ_N. Hence the computational domain Ω is an annulus of thickness $t = R - a = 5\lambda$. Table 2 summarizes the L_2 error corresponding to the DtN and BGT2 boundary conditions, for different wave numbers. At low wave numbers, both boundary conditions perform well as they lead to similar low L_2 error. In this case, the thickness t of the computational domain is large in term of the scatterer's radius a ($t/a = 5$ for $ka = 2\pi$ and $t/a = 2.5$ for $ka = 4\pi$). However, at large wave numbers, the DtN boundary condition continues to perform well while the error corresponding to BGT2 starts to deteriorate. In this case, the thickness t becomes a fraction of the radius a ($t/a = 0.5$ for $ka = 20\pi$ and $t/a = 1/3$ for $ka = 30\pi$). The BGT2 boundary condition

Table 2
L_2 error corresponding to DtN and BGT2 boundary conditions on Γ_R.

$ka = 2\pi, R/a = 6$			$ka = 4\pi, R/a = 3.5$			$ka = 8\pi, R/a = 2$			$ka = 20\pi, R/a = 1.5$			$ka = 30\pi, R/a = 1.333\ldots$		
τ	ϵ_2 [%] DtN	ϵ_2 [%] BGT2	τ	ϵ_2 [%] DtN	ϵ_2 [%] BGT2	τ	ϵ_2 [%] DtN	ϵ_2 [%] BGT2	τ	ϵ_2 [%] DtN	ϵ_2 [%] BGT2	τ	ϵ_2 [%] DtN	ϵ_2 [%] BGT2
3.1	1.87	1.75	3.0	1.00	0.92	3.1	0.81	0.82	3.0	0.14	1.03	3.0	0.09	1.98
3.3	0.56	0.56	3.2	0.62	0.70	3.4	0.29	0.39	3.3	0.23	1.02	3.3	0.08	1.98
3.6	0.38	0.36	3.6	0.30	0.30	3.6	0.28	0.38	3.6	0.05	1.02	3.6	0.07	1.98

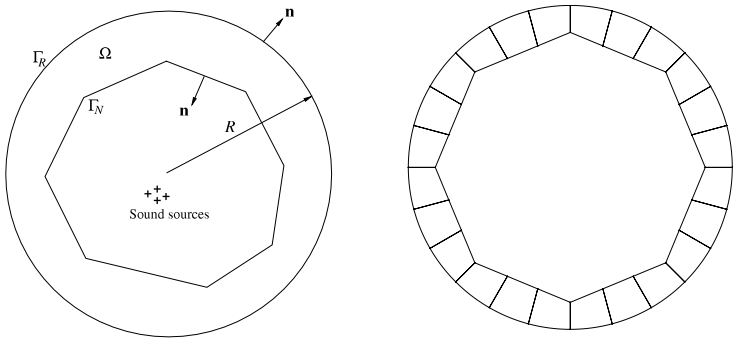

Fig. 3. Interfering sound sources inside a polygon shaped window: (left) schematic diagram, (right) mesh of the computational domain.

performs well up to a thickness of the annulus Ω equal to the scatterer's radius; that is $t/a = 1$ for $ka = 8\pi$. For $t/a < 1$, the BGT2 L_2 error starts to increase.

In all computations, most of the CPU time was dedicated to the evaluation of the oscillatory integrals resulting from the products of plane waves. This is true particularly at high wave numbers where large numbers of integration points are used. Consequently, the solution time is only a fraction of the time required during the process of matrix assembly. Moreover, the computational time of the PUFEM-DtN model is slightly higher than the time required when approximate NRBCs are used. This is due to the DtN operator being non-local.

For the plane wave scattering problem solved above, the inner boundary of the computational domain is circular and hence the outward normal vector is continuous throughout the whole boundary. In the following numerical experiment, a test problem is briefly presented in which the outward normal to the inner boundary Γ_N is discontinuous. Consider the solution of a wave problem in an unbounded domain due to the interference of various sound sources. The domain of interest Ω is bounded by an external circular boundary Γ_R of radius R, on which the DtN boundary condition is used, and by an internal polygon shaped boundary Γ_N, on which the normal velocity of the interfering sources is specified (Fig. 3 (left)). This technique which consists of imposing a known normal velocity on the inner boundary was used in [36] to assess the stability of infinite element schemes for transient wave problems. In practical applications, the problem inside Γ_N may involve sound sources and reflecting surfaces of general shapes. For such cases, it is difficult to assess the accuracy of the results as analytical solutions are not available.

For the interference test problem considered here, the equivalent variational formulation to (5) is given by

$$\int_{\Omega} \left(\nabla u \cdot \nabla v - k^2 uv\right) \mathrm{d}\Omega - \int_{\Gamma_R} vBu \,\mathrm{d}\Gamma_R = \int_{\Gamma_N} v \nabla w \cdot \boldsymbol{n} \,\mathrm{d}\Gamma, \tag{19}$$

where w is representing the sound sources inside Γ_N. As an example, 4 radial sound sources placed at different locations are considered to interfere. The computational domain Ω is limited by an inner boundary in the shape of a regular octagon and an outer circular boundary. It is meshed into 24 elements with 9 nodes each (Fig. 3 (right)). The function w is given by the sum of Hankel functions of first kind and order zero with sources located at radii $\boldsymbol{r}_j$. That is $w = \sum_{j=1}^{4} H_0(k|\boldsymbol{r} - \boldsymbol{r}_j|)$, with $\boldsymbol{r}_j = (0.3, 0.3)^{\mathrm{T}}$, $(-0.3, 0.3)^{\mathrm{T}}$, $(-0.3, -0.3)^{\mathrm{T}}$ and $(0.3, -0.3)^{\mathrm{T}}$ for $j = 1, 2, 3$ and 4, respectively. The L_2 error of the solution is obtained from the expression previously defined where $\tilde{u}$ is replaced by w. This test example is run for two extreme cases of the wave number $ka = 10$ and $ka = 120$, and under similar conditions of the scattering problem solved earlier regarding the number of plane waves attached at each node, the number of integration points and the number of components in the DtN series. The only difference lies in the geometry of the computational domain which is bounded by an inner octagonal boundary Γ_N with corners placed at a unit distance a from the center and the outer circular boundary Γ_R placed at $R/a = 1.2$.

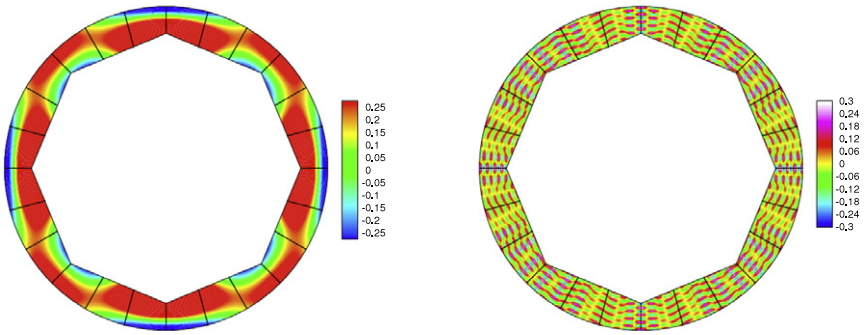

Fig. 4. Sound sources inside a polygon shaped window, real part of the potential: (left) $ka = 10$, $\tau = 32$, $\epsilon_2 = 0.007\%$, (right) $ka = 120$, $\tau = 2.6$, $\epsilon_2 = 0.8\%$.

Fig. 4 shows the real part of the potential throughout the computational domain. For $ka = 10$, the outer boundary is around $\lambda/3$ away from the corners of the octagon. The L_2 error is very low, $\epsilon_2 = 0.007\%$, and is due to the use of many more DOF per wavelength than usually required, $\tau = 32$. For $ka = 120$, the outer boundary is about 4λ away from the corners of the octagon. The L_2 error shows a very good accuracy of the results, $\epsilon_2 = 0.8\%$, for a discretization level of only 2.6 DOF per wavelength.

5. Conclusion

In this work, a wave scattering problem is solved with a fixed mesh for a wide range of wave numbers. The used PUFEM model allows to compute many wavelengths per nodal spacing provided that enough integration points are used in the evaluation of the element matrices. The numerical results show that the combined model PUFEM-DtN provides accurate results even when the outer boundary of the computational domain is very close to the scatterer. Regarding approximate NRBCs, it is found that, at low wave numbers, BGT2 is more accurate than EM2, F2 and F3. However, at high wave numbers, they all lead to similar accuracy. Moreover, at high wave numbers, when the outer boundary is very close to the scatterer in term of the absolute distance, but many wavelengths away from it, approximate NRBCs perform poorly. This is due to the fact that approximate radiation conditions are based on asymptotic expansions and hence are not valid in the immediate surrounding of the scattering object. It seems that approximate NRBCs lead to optimal results when the outer boundary is placed at a distance equal to the radius of the scattering object.

The DtN operator, compared with the approximate NRBCs for identical computational domains, leads to better accuracy results. However, it is more demanding at the implementation level because of its non-local nature. As a consequence, it leads to higher computational effort during the integration along the outer boundary and during the solution process. But this does not mean that the DtN model is computationally more expensive. In fact, a model using approximate NRBCs would be computationally more expensive than a model using the DtN if the same accuracy is sought, because the former would require a much larger domain. Therefore, the choice of the best option between PUFEM-DtN and PUFEM-approximate NRBCs must be based on practical considerations; either go for a reduced computational domain with a global matrix dense near the outer boundary, for PUFEM-DtN, or choose a larger computational domain with a sparse global matrix, for PUFEM-approximate NRBCs.

Last, it should be possible to extend the combined model of PUFEM-DtN to three dimensions, in which case many real problems could be solved with a significantly reduced computational domain. It is believed that by meshing the computational domain with a single layer of multi-wavelength sized finite elements around the scatterer, this will reduce the size of the global matrix and lead to solutions of 3D problems for a wide range of wave numbers with a reasonable computing effort.

Acknowledgements

The first author is grateful to the Royal Society and the Nuffield Foundation for funding the research computing facilities. The Carnegie Trust for the Universities of Scotland is acknowledged for supporting travel and subsistence for collaboration. We are also grateful to Professor Jeremy Astley for very useful discussions.

References

[1] J.M. Melenk, I. Babuška, The partition of unity finite element method. Basic theory and applications, Comput. Methods Appl. Mech. Engrg. 139 (1996) 289–314.
[2] I. Babuška, J.M. Melenk, The partition of unity method, Internat. J. Numer. Methods Engrg. 40 (1997) 727–758.
[3] O. Laghrouche, P. Bettess, Short wave modelling using special finite elements, J. Comput. Acoust. 8 (1) (2000) 189–210.
[4] P. Ortiz, E. Sanchez, An improved partition of unity finite element model for diffraction problems, Internat. J. Numer. Methods Engrg. 50 (2001) 2727–2740.

[5] R.J. Astley, P. Gamallo, Special short wave elements for flow acoustics, Comput. Methods Appl. Mech. Engrg. 194 (2005) 341–353.
[6] P. Monk, D.Q. Wang, A least-squares method for the Helmholtz equation, Comput. Methods Appl. Mech. Engrg. 175 (1999) 121–136.
[7] O. Cessenat, B. Després, Application of an ultra weak variational formulation of elliptic PDEs to the two-dimensional Helmholtz problem, SIAM J. Numer. Anal. 35 (1) (1998) 255–299.
[8] T. Huttunen, P. Monk, J.P. Kaipio, Computation aspects of the ultra weak variational formulation, J. Comput. Phys. 182 (2002) 27–46.
[9] C. Farhat, I. Harari, L. Franca, The discontinuous enrichment method, Comput. Methods Appl. Mech. Engrg. 190 (2001) 6455–6479.
[10] C. Farhat, I. Harari, U. Hetmanuk, A discontinuous Galerkin method with Lagrange multipliers for the solution of Helmholtz problems in the mid-frequency regime, Comput. Methods Appl. Mech. Engrg. 192 (2003) 1389–1419.
[11] P. Bettess, O. Laghrouche, E. Perrey-Debain (Eds.), Theme issue on short wave scattering, Philos. Trans. R. Soc. Lond. A 362 (2004).
[12] O. Laghrouche, P. Bettess, E. Perrey-Debain, J. Trevelyan, Wave interpolation finite elements for Helmholtz problems with jumps in the wave speed, Comput. Methods Appl. Mech. Engrg. 194 (2005) 367–381.
[13] T. Strouboulis, I. Babuška, R. Hidajat, The generalized finite element method for Helmholtz equation: Theory, computation, and open problems, Comput. Methods Appl. Mech. Engrg. 195 (2006) 4711–4731.
[14] O. Laghrouche, P. Bettess, Short wave modelling using special finite elements Towards an adaptive approach, in: J.R. Whiteman (Ed.), Mathematics of Finite Elements and Applications, Elsevier, 2000, pp. 181–194 (chapter 10).
[15] O. Laghrouche, P. Bettess, R.J. Astley, Modelling of short wave diffraction problems using approximating systems of plane waves, Internat. J. Numer. Methods Engrg. 54 (2002) 1501–1533.
[16] E. Perrey-Debain, O. Laghrouche, P. Bettess, J. Trevelyan, Plane wave basis finite lements and boundary elements for three dimensional wave scattering, Philos. Trans. R. Soc. Lond. A 362 (2004) 561–577.
[17] A. Bayliss, E. Turkel, Radiation boundary conditions for wave-like equations, Commun. Pure Appl. Math. 33 (1980) 707–725.
[18] A. Bayliss, M. Gunzburger, E. Turkel, Boundary conditions for the numerical solution of elliptic equations in exterior regions, J. Appl. Math. 42 (1982) 430–451.
[19] B. Engquist, A. Majda, Absorbing boundary conditions for the numerical simulation of waves, Math. Comput. 31 (1977) 629–651.
[20] B. Engquist, A. Majda, Radiation boundary conditions for acoustic and elastic wave calculations, Commun. Pure Appl. Math. 32 (1979) 313–357.
[21] F. Kang, Finite element method and natural boundary reduction, in: Proceedings of the International Congress of Mathematics, Warsaw, 1983, 1439–1453.
[22] J.B. Keller, D. Givoli, Exact non-reflecting boundary conditions, J. Comput. Phys. 82 (1989) 172–192.
[23] M.J. Grote, C. Kirsch, Dirichlet-to-Neumann boundary conditions for multiple scattering problems, J. Comput. Phys. 201 (2004) 630–650.
[24] D. Givoli, Numerical Methods for Problems in Infinite Domains, Elsevier Science Publishers, Amsterdam, 1992.
[25] D. Givoli, Recent advances in the DtN F E Method, Arch. Comput. Methods Engrg. 6 (1999) 71–116.
[26] M.J. Grote, J.B. Keller, On nonreflecting boundary conditions, J. Comput. Phys. 122 (1995) 231–243.
[27] I. Harari, T.J.R. Hughes, Analysis of continuous formulations underlying the computation of time-harmonic acoustics in exterior domains, Comput. Methods Appl. Mech. Engrg. 97 (1992) 103–124.
[28] I. Harari, K. Grosh, T.J.R. Hughes, M. Malhotra, P.M. Pinsky, J.R. Stewart, L.L. Thompson, Recent developments in finite element methods for structural acoustics, Arch. Comput. Methods Engrg. 3 (1996) 131–311.
[29] R.A. Adams, Sobolev Spaces, Academic Press, New York, 1975.
[30] D. Gilbarg, N.S. Trudinger, Elliptic Partial Differential Equations of Second Order, Springer-Verlag, 1983.
[31] R. Leis, Boundary Value Problems in Mathematical Physics, Teubner, Wiley, 1989.
[32] P. Bettess, J. Shirron, O. Laghrouche, B. Peseux, R. Sugimoto, J. Trevelyan, A numerical integration scheme for special finite elements for Helmholtz equation, Internat. J. Numer. Methods Engrg. 56 (2003) 531–552.
[33] P.M. Morse, H. Feshbach, Methods of Theoretical Physics, McGraw-Hill Book Company, USA, 1953.
[34] J.J. Shirron, Numerical Solution of Exterior Helmholtz Problems Using Finite and Infinite Elements, Ph.D. Thesis, College Park, MD, 1995.
[35] J.J. Shirron, I. Babuška, A comparison of approximate boundary conditions and infinite element for exterior Helmholtz problems, Comput. Methods Appl. Mech. Engrg. 164 (1998) 121–139.
[36] R.J. Astley, J.A. Hamilton, The stability of infinite element schemes for transient wave problems, Comput. Methods Appl. Mech. Engrg. 195 (2006) 3553–3571.